Dalton Transactions

ROYAL SOCIETY OF CHEMISTRY

PAPER

View Article Online
View Journal | View Issue

Cite this: *Dalton Trans.*, 2024, **53**, 7303

Inorganic–organic hybrid Cu–dipyridyl semiconducting polymers based on the redox-active cluster $[SFe_3(CO)_9]^{2-}$: filling the gap in iron carbonyl chalcogenide polymers†

Ming-Chi Hsu,[a] Ru Yan Lin,[a] Tzu-Yen Sun,[a] Yu-Xin Huang,[a] Min-Sian Li,[a] Yu-Huei Li,[a] Hui-Lung Chen*[b] and Minghuey Shieh *[a]

Received 27th January 2024,
Accepted 24th March 2024

DOI: 10.1039/d4dt00254g

rsc.li/dalton

The construction of sulfur-incorporated cluster-based coordination polymers was limited and underexplored due to the lack of efficient synthetic routes. Herein, we report facile mechanochemical ways toward a new series of $SFe_3(CO)_9$-based dipyridyl–Cu polymers by three-component reactions of $[Et_4N]_2[SFe_3(CO)_9]$ ($[Et_4N]_2$[**1**]) and $[Cu(MeCN)_4][BF_4]$ with conjugated or conjugation-interrupted dipyridyl ligands, 1,2-bis(4-pyridyl)ethylene (bpee), 1,2-bis(4-pyridyl)ethane (bpea), 4,4′-dipyridyl (dpy), or 1,3-bis(4-pyridyl)propane (bpp), respectively. X-ray analysis showed that bpee-containing 2D polymers demonstrated unique $SFe_3(CO)_9$ cluster-armed and cluster-one-armed coordination modes *via* the hypervalent μ_5-S atom. These S–Fe–Cu polymers could undergo flexible structural transformations with the change of cluster bonding modes by grinding with stoichiometric amounts of dipyridyls or **1**/$[Cu(MeCN)_4]^+$. They exhibited semiconducting behaviors with low energy gaps of 1.55–1.79 eV and good electrical conductivities of 3.26×10^{-8}–1.48×10^{-6} S cm^{-1}, tuned by the $SFe_3(CO)_9$ cluster bonding modes accompanied by secondary interactions in the solid state. The electron transport efficiency of these polymers was further elucidated by solid-state packing, X-ray photoelectron spectroscopy (XPS), X-ray absorption near-edge spectroscopy (XANES), density of states (DOS), and crystal orbital Hamilton population (COHP) analysis. Finally, the solid-state electrochemistry of these polymers demonstrated redox-active behaviors with cathodically-shifted patterns compared to that of $[Et_4N]_2$[**1**], showing that their efficient electron communication was effectively enhanced by introducing **1** and dipyridyls as hybrid ligands into Cu^+-containing networks.

Introduction

Metal cluster-based coordination frameworks have gained much attention due to their fascinating structures and intriguing physical and chemical properties.[1,2] Metal clusters can act as nodes or inorganic ligands which could couple with organic multidentate ligands to construct inorganic–organic hybrid polymeric structures.[1,2] Several reports have shown that metal carbonyl clusters could be used as secondary building units,[1,2] in which CO ligands effectively modulated the electronic structures and served as hydrogen bond acceptors within the frameworks. As a consequence, these metal carbonyl cluster-based polymers showed potential applications in catalysis, host–guest chemistry, and semiconductors.[2]

In recent decades, research on main-group-introduced carbonyl clusters has grown significantly.[3] Main group elements can provide s/p hybridization to couple with the d orbitals of transition metals, leading to the unique structures and special properties of the resultant clusters. Studies on main group element-incorporated metal carbonyl cluster-based polymers were largely focused on groups 15 and 16 element-containing systems, in which clusters $Pn_2Mo_2(CO)_4Cp_2$ (Pn = P, As, and Sb)[4] and $[EFe_3(CO)_9]^{2-}$ (E = Te, Se)[5] serving as building units to construct 1D to 3D frameworks were most reported.

Recently, our group has developed $EFe_3(CO)_9$-based (E = Te, Se) 1D and 2D Cu polymers, which could be synthesized from the pre-designed clusters $[EFe_3(CO)_9\{Cu(MeCN)\}_2]$ (E = Te, Se) or $[SeFe_3(CO)_9]^{2-}$/$[Cu(MeCN)_4]^+$ in the presence or absence of organic ligands.[5a–e] Numerous bonding modes of clusters $EFe_3(CO)_9$ (E = Te, Se) in their Cu–dipyridyl polymers were found, and they were classified as the linking (**L**), blocking (**B**),

[a]*Department of Chemistry, National Taiwan Normal University, Taipei 116325, Taiwan, Republic of China. E-mail: mshieh@ntnu.edu.tw*
[b]*Department of Chemistry and Institute of Applied Chemistry, Chinese Culture University, Taipei 111396, Taiwan, Republic of China. E-mail: chl3@faculty.pccu.edu.tw*

†Electronic supplementary information (ESI) available. CCDC 2321671–2321676. For ESI and crystallographic data in CIF or other electronic format see DOI: https://doi.org/10.1039/d4dt00254g

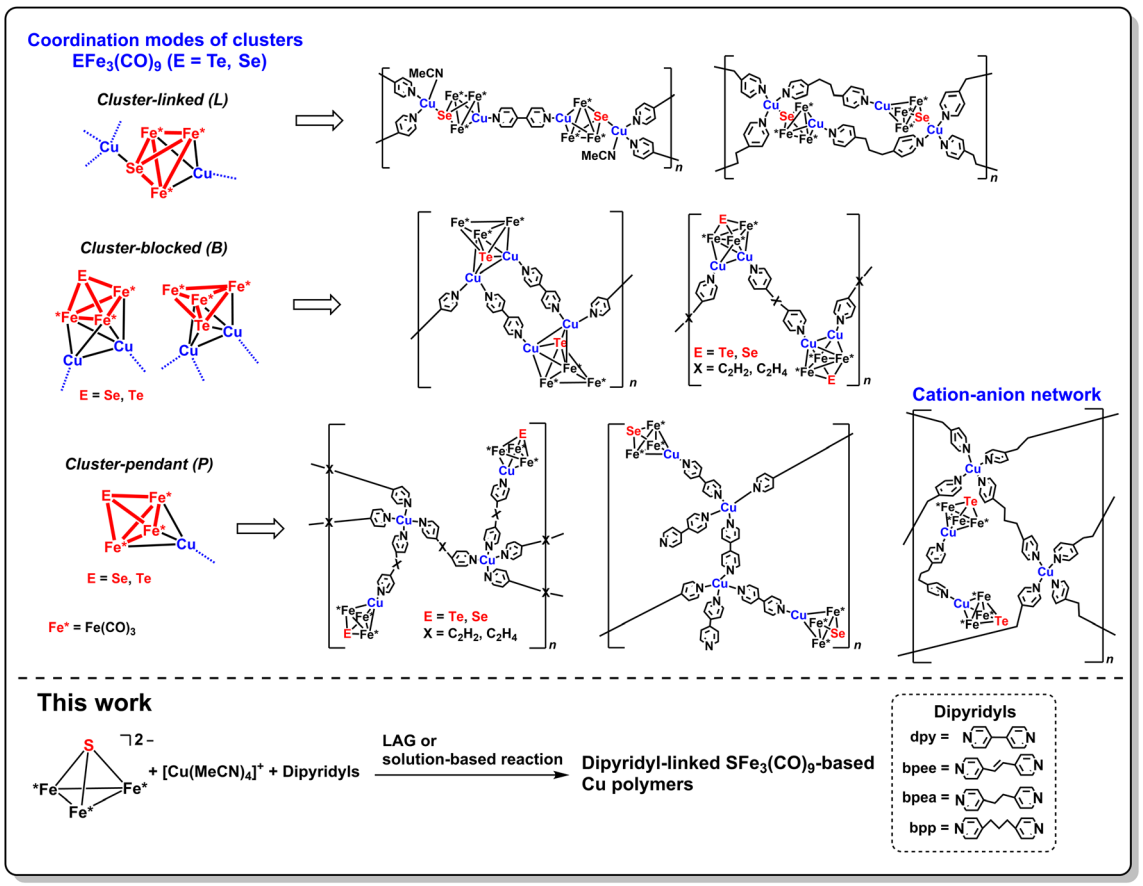

Scheme 1 The reported $EFe_3(CO)_9$-based (E = Te, Se) dipyridyl-linked Cu polymers with various coordination modes of $EFe_3(CO)_9$.

or pendant (**P**) inorganic ligands within the frameworks (Scheme 1).[5a–c] It was also noted that the semiconductivities and photodegradation abilities of these $EFe_3(CO)_9$-based (E = Te, Se) polymers could be fine-tuned by the versatile coordination modes and secondary weak interactions in the solid state.[5a–c]

In addition to the above-mentioned Te- and Se-containing polymers, to fill the gap in the chalcogen iron carbonyl cluster-based polymers, we will focus on lighter sulfur systems in this study. Introducing the sulfur atom into the $SFe_3(CO)_9$ cluster as the inorganic ligand for polymeric frameworks was believed to provide better orbital overlap with the transition metal node, giving rise to unexpected polymeric structures with better electron communications.

In the present work, we applied a three-component liquid-assisted grinding (LAG)[6] or solution-based method to synthesize a novel family of $SFe_3(CO)_9$-based Cu–dipyridyl polymers. These newly synthesized polymers exhibited versatile structural features with unique $SFe_3(CO)_9$ coordination modes, and their reversible inter-structural transformations were also achieved by the addition of organic ligands, inorganic clusters, or metal nodes. These S-containing polymers showed surprising semiconducting behaviors, in which their electron communication efficiency was rationalized by the $SFe_3(CO)_9$ coordination modes with numerous secondary interactions in the solid state, as evidenced by solid-state packing, diffuse reflectance spectroscopy, electrical conductivity measurement, X-ray photoelectron spectroscopy, X-ray absorption near-edge structure analysis, and DFT calculations. For practical use, the redox behaviors of these $SFe_3(CO)_9$-based polymers were investigated by solid-state electrochemistry.

Results and discussion

Syntheses and structural transformations of inorganic–organic hybrid S–Fe–Cu–CO polymers containing the rigid bpee or flexible bpea ligand

With success achieved in the preparation of $Te/SeFe_3(CO)_9$ cluster-based polymers *via* LAG,[5a,b] we applied three-component LAG synthetic routes to a series of $SFe_3(CO)_9$–dipyridyl hybrid Cu polymers, first starting from rigid conjugated 1,2-bis(4-pyridyl)ethylene (bpee) or flexible non-conjugated 1,2-bis(4-pyridyl)ethane (bpea) as the organic linker (Scheme 2).

As shown in Scheme 2, when a mixture of clusters $[Et_4N]_2[SFe_3(CO)_9]$ ($[Et_4N]_2$[**1**]) and $[Cu(MeCN)_4][BF_4]$ with one equivalent of bpea or bpee was ground with few drops of THF/Et_2O or THF, the cluster-blocked (**B**) 1D zig-zag chain polymers $[(\mu_3\text{-}S)Fe_3(CO)_9Cu_2(L)]_n$ (**1-L-1D**, L = bpea, bpee) were formed, respectively. Their structures and formulations were confirmed

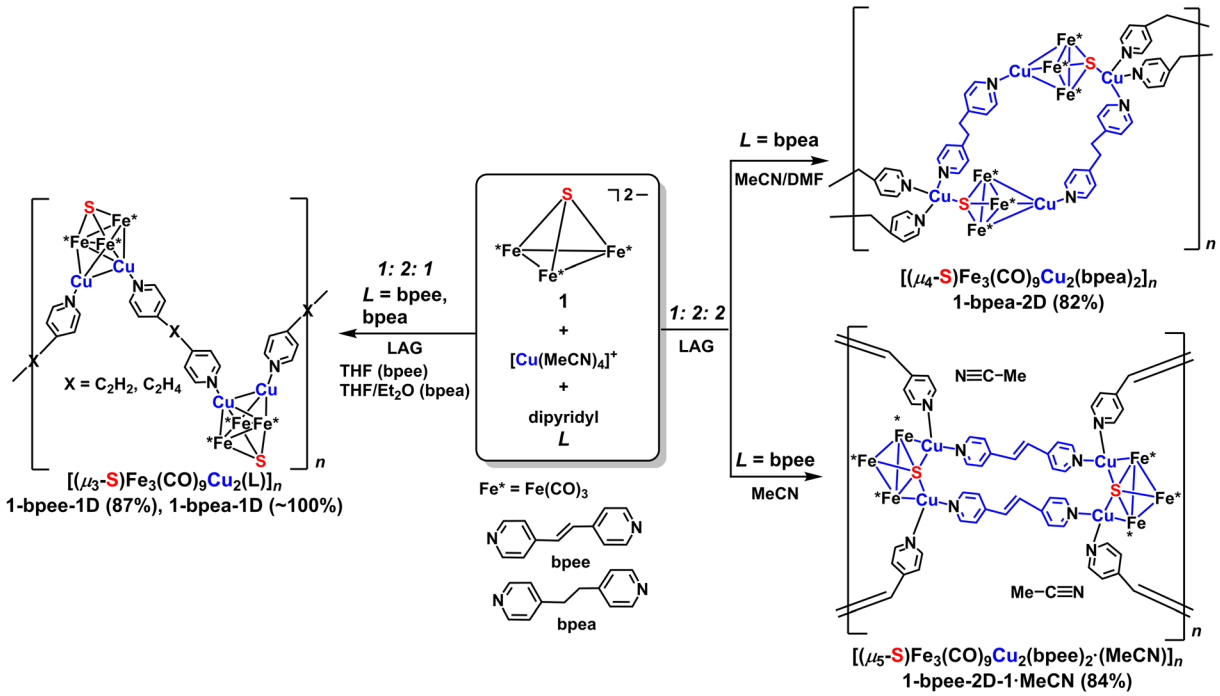

Scheme 2 LAG syntheses of S–Fe–Cu polymers with low equivalents of bpee and bpea ligands.

by powder X-ray diffraction (PXRD) and elemental analysis, in which the experimental PXRD patterns were similar to those of the simulated ones based on the published 1D structures $[(\mu_3\text{-Te})Fe_3(CO)_9Cu_2(L)]_n$ (L = bpea, bpee) (Fig. S1†).[5b] Similarly, these 1D polymers **1-L-1D** (L = bpea, bpee) contained Cu–Cu-bonded $SFe_3(CO)_9Cu_2$ cores that were connected by dipyridyls to form 1D zig-zag chains. Furthermore, if the LAG reactions were performed with two equivalents of bpea or bpee, the molecular loop-containing 2D polymers $[(\mu_4\text{-S})Fe_3(CO)_9Cu_2(bpea)_2]_n$ (**1-bpea-2D**) and $[(\mu_5\text{-S})Fe_3(CO)_9Cu_2(bpee)_2]_n$ (**1-bpee-2D-1**) were obtained in high yields (Scheme 2 and Fig. 1a). Crystals of **1-bpea-2D** and **1-bpee-2D-1·MeCN** were obtained from the crystallization of as-synthesized powders in MeCN/DMF and MeCN, respectively. The experimental PXRD pattern of **1-bpea-2D** was consistent with the simulated one based on data from single-crystal structure analysis (Fig. 1a). The experimental PXRD pattern of the ground sample of **1-bpee-2D-1**, easy loss of the lattice solvent MeCN, was similar but shifted to higher angles based on the simulation of single-crystal data of **1-bpee-2D-1·MeCN** (Fig. 1a). It was also found that the ground powder **1-bpee-2D-1** could be converted back to the MeCN-solvated crystals of **1-bpee-2D-1·MeCN** by slow crystallization in MeCN. Thus, the main framework of **1-bpee-2D-1** was considered the same as that of **1-bpee-2D-1·MeCN**.

Polymer **1-bpea-2D** consisted of flexible $[\{(\mu_4\text{-S})Fe_3(CO)_9Cu_2(bpea)\}_2]$ molecular loops which were connected by bpea *via* Cu atoms to give a 2D plane network (Fig. 2a and

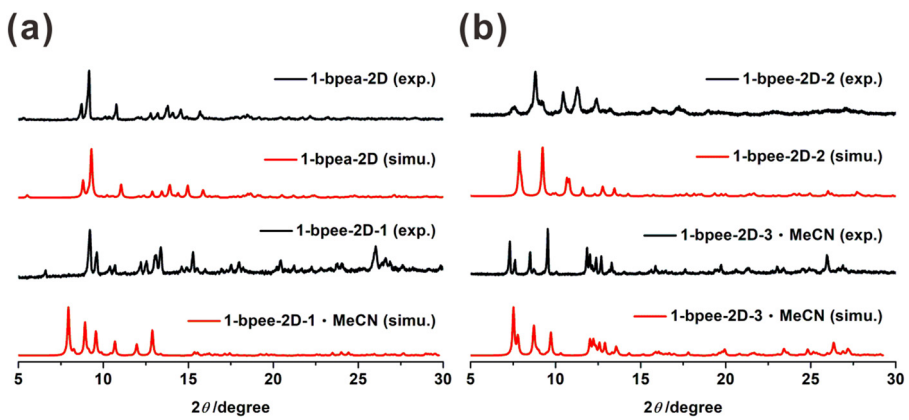

Fig. 1 Experimental (black) and simulated (red) PXRD spectra of (a) **1-bpea-2D** and **1-bpee-2D-1** and (b) **1-bpee-2D-2** and **1-bpee-2D-3·MeCN**.

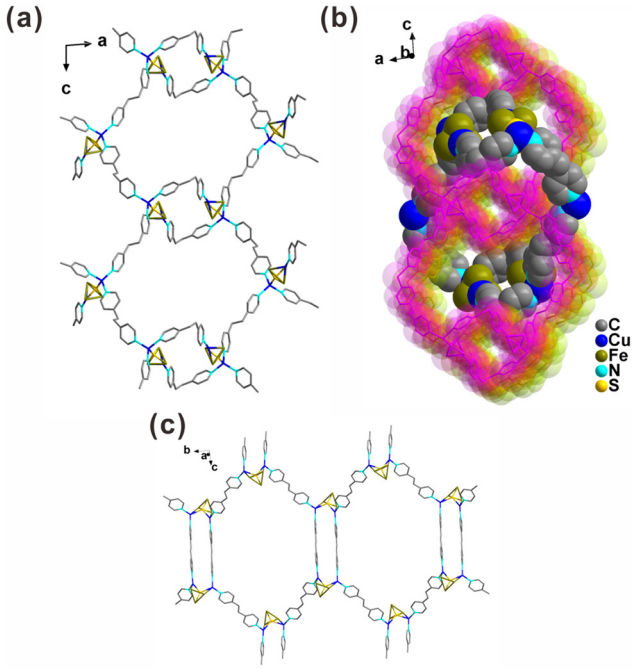

Fig. 2 Portions of polymeric frameworks of (a) **1-bpea-2D**, (b) four-fold interpenetrated network of **1-bpea-2D**, and (c) **1-bpee-2D-1·MeCN**. CO, H, and solvated MeCN have been omitted for clarity.

S5†). The cluster $SFe_3(CO)_9$ moieties of polymer **1-bpea-2D** were coordinated to Cu metals through the S vertex and Fe_3 ring, designated as a cluster-linked (**L**) coordination mode. Notably, the 2D networks of polymer **1-bpea-2D** were further interpenetrated to give rise to a four-fold interpenetrated network (Fig. 2b). For polymer **1-bpee-2D-1·MeCN**, each of the repeating units contained a rigid dicluster-based molecular loop $[\{(\mu_5\text{-S})Fe_3(CO)_9Cu_2(bpee)\}_2]$ with parallel-displaced bpee ligands, in which the Cu nodes were further connected by bpee ligands to produce a 2D framework (Fig. 2c and S5†). The $SFe_3(CO)_9$ cluster moieties in **1-bpee-2D-1·MeCN** were coordinated to Cu atoms *via* the Fe–S–Fe chain, a so-called cluster-armed (**A**) coordination mode which was first seen in the chalcogen-containing iron carbonyl Cu–dipyridyl polymers.

As the reactions proceeded with increased stoichiometric amounts of the bpee ligand to 3 or 3.5 equivalents, two novel 2D polymers $[(\mu_5\text{-S})Fe_3(CO)_9Cu_2(bpee)_3]_n$ (**1-bpee-2D-2**) and $[(\mu_5\text{-S})Fe_3(CO)_9Cu_2(bpee)_{3.5}\cdot MeCN]_n$ (**1-bpee-2D-3·MeCN**) were produced in good yields *via* a solution-based or LAG reaction, respectively (Scheme 3 and Fig. 1b). Similar reactions failed in the bpea system, probably due to the flexibility of the saturated C_2 bridging moiety in bpea. Crystals of **1-bpee-2D-2** and **1-bpee-2D-3·MeCN** suitable for X-ray diffraction were grown in MeCN solutions, and their experimental PXRD spectra were consistent with the simulated ones based on the crystallographic data. Polymer **1-bpee-2D-2** contained dicluster-based molecular loop $[\{(\mu_5\text{-S})Fe_3(CO)_9Cu_2bpee\}_2]$ repeating units that were linked by bpee ligands with the pendant bpee to form a 2D network (Fig. 3a). In contrast, polymer **1-bpee-2D-3·MeCN** consisted of tri-bpee-di-$SFe_3(CO)_9Cu_2$-involved "S"-like repeating units $[\{(\mu_5\text{-S})Fe_3(CO)_9Cu_2\}_2bpee_3]$ that were further connected by bpee ligands *via* Cu nodes with the pendant bpee to give a 2D network (Fig. 3b). The bpee ligands within the molecular loop or the "S"-like structure were parallelly aligned in the solid state (Fig. 3). Similar but different to the cluster-armed polymer **1-bpee-2D-1·MeCN**, polymers **1-bpee-2D-2** and **1-bpee-2D-3·MeCN** displayed the so-called cluster-one-armed (**OA**) coordination mode with one missing Cu–Fe bond (Fig. S5†).

To explore the structural reversibility of these synthesized polymers, we investigated their structural transformations *via* LAG. As shown in Scheme 4a and Fig. S2,† reversible dimensionality structural transformations between polymers **1-bpea-1D** and **1-bpea-2D** were accomplished by treating them with stoichiometric amounts of bpea or **1**/$[Cu(MeCN)_4]^+$, respectively. For bpee-containing polymers **1-bpee-2D-*n*** (n = 1–3),

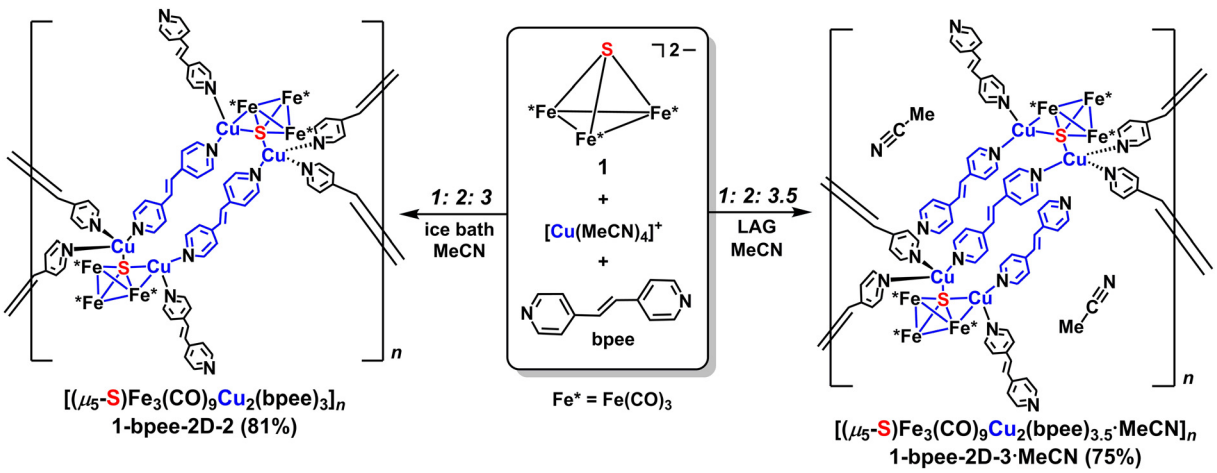

Scheme 3 Syntheses of S–Fe–Cu polymers with high equivalents of the bpee ligand.

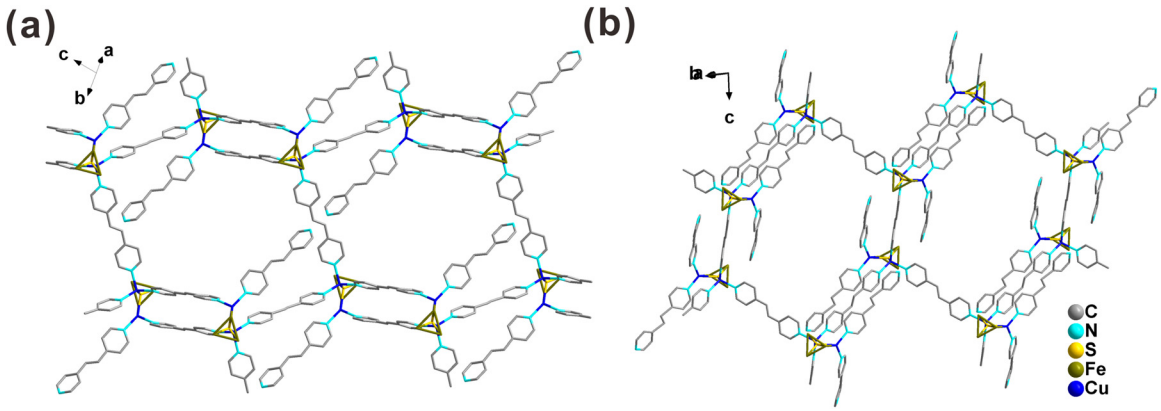

Fig. 3 Portions of the polymeric frameworks of (a) **1-bpee-2D-2** and (b) **1-bpee-2D-3·MeCN**. CO, H, and solvated MeCN have been omitted for clarity.

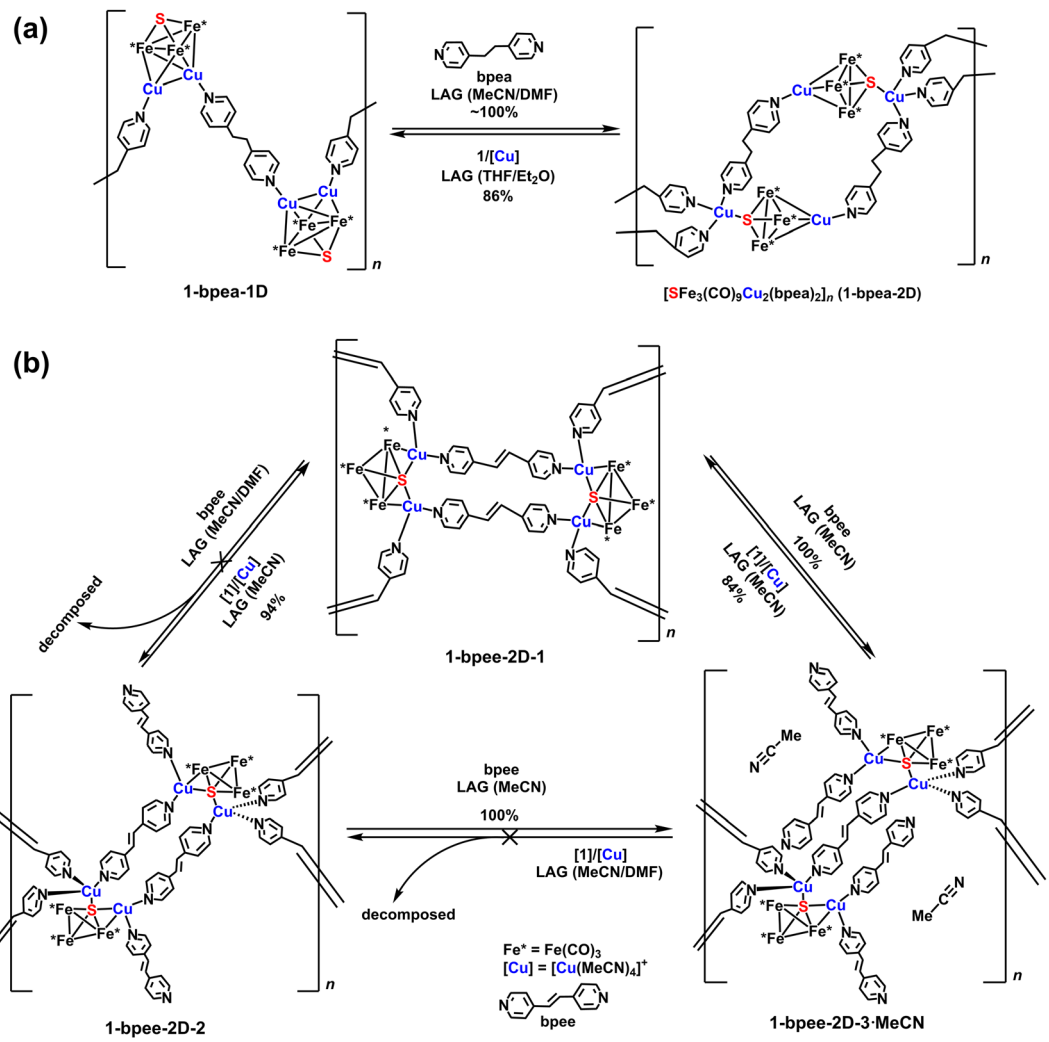

Scheme 4 Structural transformations of (a) bpea- and (b) bpee-containing polymers *via* LAG.

their reversible structural transformations succeeded between **1-bpee-2D-1** and **1-bpee-2D-3·MeCN** upon grinding with bpee or **1**/$[Cu(MeCN)_4]^+$ (Scheme 4b and Fig. S3†), and the transformation from polymer **1-bpee-2D-2** to **1-bpee-2D-1** or to **1-bpee-2D-3·MeCN** was achieved by adding **1**/$[Cu(MeCN)_4]^+$ or bpee (Scheme 4b and Fig. S4†). Based on these results, the

controllable stepwise structural transformations of these bpea- and bpee-based polymers were facilely attained by the addition of appropriate amounts of dipyridyls or **1**/$[Cu(MeCN)_4]^+$ components.

Syntheses and structural transformations of S–Fe–Cu–CO polymers containing the conjugated dpy or conjugation-interrupted bpp ligand

For a better comparison, the $SFe_3(CO)_9$-based three-component LAG reactions were also conducted on 4,4′-dipyridyl (dpy) and 1,3-bis(4-pyridyl)propane (bpp) systems. As a result, the $SFe_3(CO)_9$-linked (**L**) dpy-connected 2D polymer $[(\mu_4\text{-S})Fe_3(CO)_9Cu_2(MeCN)(dpy)_{1.5}]_n$ (**1-dpy-2D**), the $SFe_3(CO)_9$-pendant (**P**) dpy-bridged 1D chain $[(\mu_3\text{-S})Fe_3(CO)_9Cu_2(dpy)_3]_n$ (**1-dpy-1D**), and the $SFe_3(CO)_9$-linked (**L**) bpp molecular loop-containing 2D polymer $[(\mu_4\text{-S})Fe_3(CO)_9Cu_2(bpp)_2]_n$ (**1-bpp-2D**) were produced upon treatment with stoichiometric amounts of cluster **1**, $[Cu(MeCN)_4]^+$, and dipyridyls (Scheme 5). X-ray analysis and PXRD data confirmed these $SFe_3(CO)_9$-based polymers **1-dpy-2D**, **1-dpy-1D**, and **1-bpp-2D** to be isostructural to those reported in the Se system.[5a]

Similar to the Se congeners,[5a] polymers **1-dpy-2D** and **1-bpp-2D** contained $[\{(\mu_4\text{-S})Fe_3(CO)_9Cu_2(MeCN)\}_2(dpy)]$ chains (Fig. S7a†) or $[\{(\mu_4\text{-S})Fe_3(CO)_9Cu_2(bpp)\}_2]$ molecular loops as building units which were connected by dipyridyls *via* outward Cu nodes to form 2D honeycomb-like networks, in which polymer **1-dpy-2D** formed a five-fold interpenetrated 2D network in the solid state (Fig. S8†). Polymer **1-dpy-1D** consisted of a Cu–dpy chain coordinated by the pendant $[SFe_3(CO)_9Cu(dpy)]$ and dpy ligands *via* Cu nodes to construct a 1D zig-zag chain (Fig. S7b†). The reversible dimensionality structural transformations between **1-dpy-2D** and **1-dpy-1D** were also noted by grinding with dpy or **1**/$[Cu(MeCN)_4]^+$, respectively (Scheme 5 and Fig. S9†).

Structural feature description

As stated above, these $SFe_3(CO)_9$-based dipyridyl–Cu polymers possessed versatile coordination modes of cluster $SFe_3(CO)_9$, in which new cluster-armed (**A**) and cluster-one-armed (**OA**) bonding patterns were discovered in bpee-containing 2D polymers (Scheme 6). The formation of these new coordination modes in sulfur-based Cu–bpee networks could be mainly attributed to the hypervalent μ_5-S atom of the inorganic cluster $SFe_3(CO)_9$, which had a better orbital overlap with Cu nodes compared to heavier Te and Se systems.[7]

Moreover, structurally characterized 2D polymers, including **1-dpy-2D** (**L**), **1-bpea-2D** (**L**), **1-bpee-2D-1·MeCN** (**A**), **1-bpee-2D-2** (**OA**), and **1-bpee-2D-3·MeCN** (**OA**), could be viewed as (6,3)-honeycomb (6^3-**hcb**)[8] networks, in which molecular loop-containing polymers **1-bpea-2D**, **1-bpee-2D-1·MeCN**, and **1-bpee-2D-2** could alternatively be regarded as molecular loop-centered $\{4^4{\cdot}6^2\}$ square lattice (**sql**)[8] networks (Fig. S10†). Solid-state packings demonstrated that these 1D and 2D polymers were closely packed *via* non-classical C–H···O(carbonyl)[9] and aromatic C–H···π[10] interactions, forming supramolecular 2D (**1-dpy-1D**) and 3D (**1-bpea-2D**, **1-bpee-2D-1·MeCN**, **1-bpee-2D-2**, **1-bpee-2D-3·MeCN**, and **1-dpy-2D**) frameworks (Fig. S11†).

Thermal stability analysis

High thermal stability is a major requirement for the use of semiconductor materials. Thus, thermogravimetric analysis (TGA) was conducted on this series of $SFe_3(CO)_9$-based polymers to study their thermal stability. As shown in Fig. S12,†

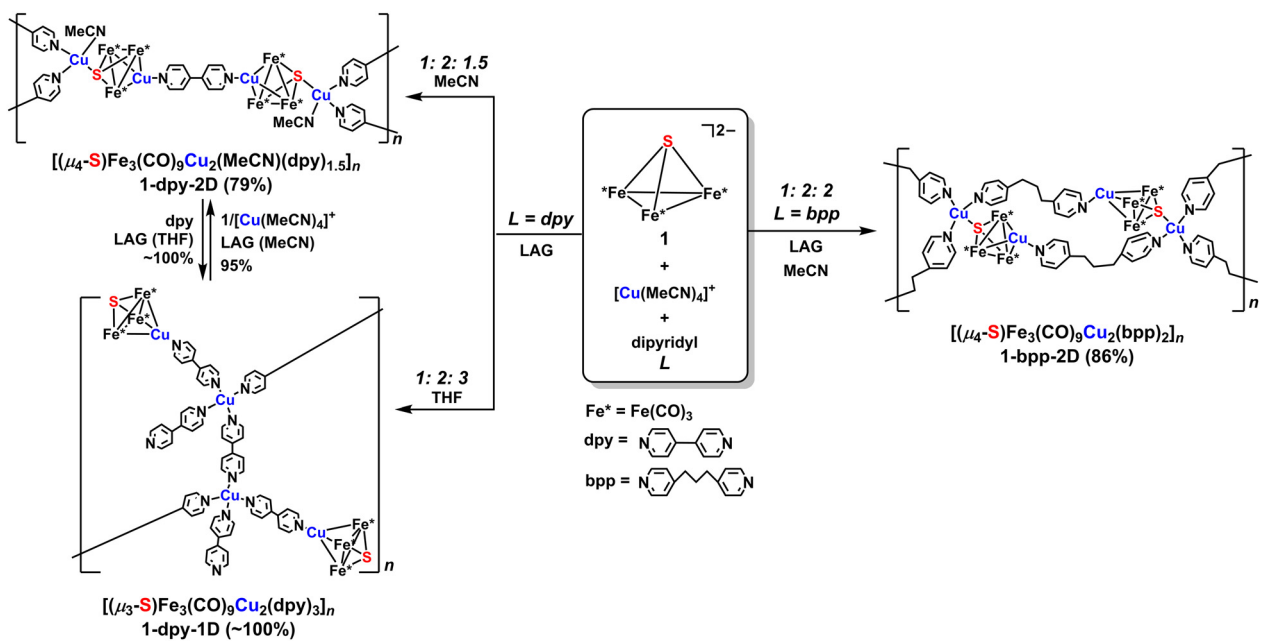

Scheme 5 Syntheses and structural transformations of the dpy- and bpp-containing S–Fe–Cu polymers *via* LAG.

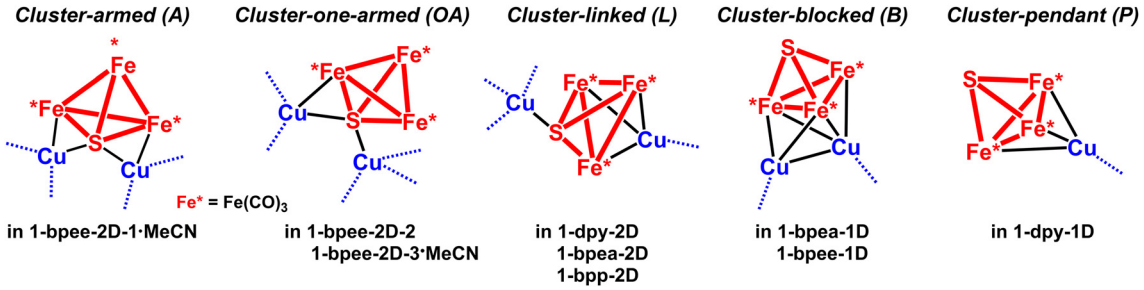

Scheme 6 Coordination modes of cluster $SFe_3(CO)_9$ in S–Fe–Cu polymers.

TGA spectra of these S–Fe–Cu polymers revealed that the weight loss began in the temperature range of 94 to 150 °C, corresponding to the release of solvated MeCN, CO ligands, and dipyridyls, which collapsed into the final $SFe_3Cu_2N_x$ (x = 0–4) residues at around 500–800 °C (Table S3†). Actually, we found that the neutral di-Cu-based cluster $[SFe_3(CO)_9\{Cu(MeCN)\}_2]$ was thermally unstable at room temperatures. Therefore, the thermal stability of these $SFe_3(CO)_9$-introduced dipyridyl Cu frameworks was significantly enhanced.

Semiconductivity studies and oxidation state determination

Cluster **1** and its derivatives showed accessible redox behaviors with low energy gaps.[2d,5d,11] Thus, to understand their semiconducting behaviors, diffuse reflectance spectroscopy and electrical conductivity of this series of $SFe_3(CO)_9$-based Cu–dipyridyl polymers were investigated. The diffuse reflectance spectra showed that the energy gap of these polymers was obtained in the range of 1.55–1.79 eV using the Kubelka–Munk function[12] (Fig. 4a and S13†). These values were significantly red-shifted from that of $[Et_4N]_2[\mathbf{1}]$ (1.87 eV),[2d] indicative of efficient electron transport by incorporating the $SFe_3(CO)_9$ cluster into Cu–dipyridyl frameworks. Interestingly, it was found that their energy gaps increased approximately in the following order of the cluster coordination modes: **L** (**1-bpea-2D**, **1-bpp-2D**, and **1-dpy-2D**, 1.55–1.61 eV), **B** (**1-bpea-1D** and **1-bpee-1D**, 1.63–1.66 eV), **OA** (**1-bpee-2D-2** and **1-bpee-2D-3·MeCN**, 1.64–1.75 eV), **A** (**1-bpee-2D-1**, 1.79 eV), and **P** (**1-dpy-1D**, 1.78 eV).

The electrical conductivity of these polymers was further measured using their pressed-pellet samples by the two-contact probe method.[13] The average electrical conductivities of these polymers lay in the range of 3.26×10^{-8}–1.48×10^{-6} S cm^{-1} (Fig. 4b and S14†),[14] consistent with the trend of their energy gaps. Most interestingly, no matter with the conjugation of dipyridyls or without it, conjugation-interrupted bpea- and bpp-connected **L**-type polymers, **1-bpea-2D** and **1-bpp-2D**, and the conjugated dpy-linked **L**-type polymer **1-dpy-2D** were found to have the best semiconductivities, indicating that efficient electron transport was significantly facilitated by the through-space C–H(dipyridyl)···O(carbonyl) and C–H(dipyridyl)···π(dipyridyl) interactions in their frameworks. In contrast, the conjugated bpee-linked **A**- and **OA**-type 2D polymers, **1-bpee-2D-1**, **1-bpee-2D-2**, and **1-bpee-2D-3·MeCN**, exhibited relatively poorer semiconductivities, likely due to the electron-trapping ability as the μ_5-S atom of $SFe_3(CO)_9$ coordinated to the Cu–dipyridyl frameworks, thus reducing the electron transport efficiency.

To gain insight into the electron communication, the oxidation state of the Cu nodes within the S–Fe–Cu polymeric frameworks was determined by X-ray photoelectron spectroscopy (XPS) and X-ray absorption near-edge spectroscopy (XANES). XPS data revealed that the Cu $2p_{3/2}$ peaks of these

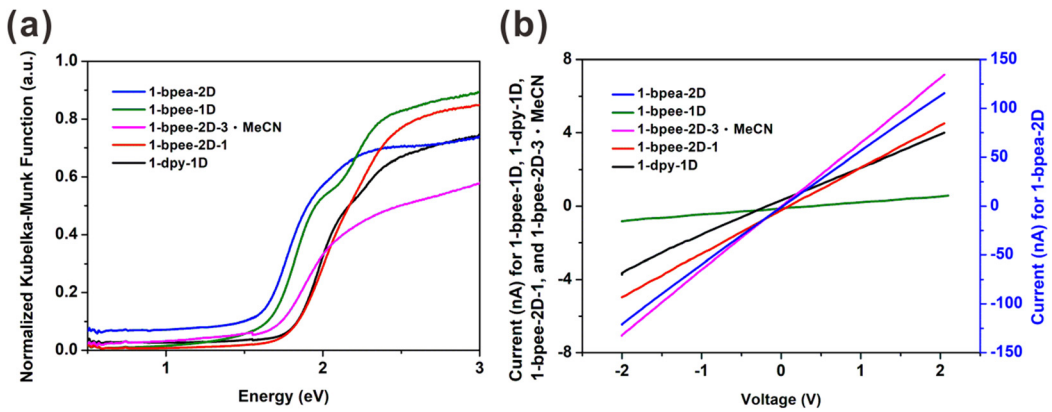

Fig. 4 (a) UV-vis diffuse reflectance spectra (plotted using the Kubelka–Munk function) and (b) I–V curves of polymers **1-bpea-2D**, **1-bpee-1D**, **1-bpee-2D-3·MeCN**, **1-bpee-2D-1**, and **1-dpy-1D**.

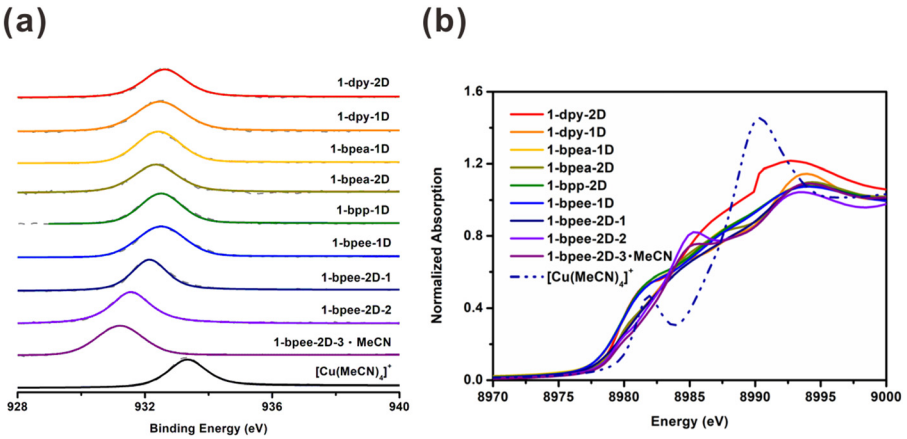

Fig. 5 (a) XPS spectra and (b) XANES spectra focusing on the Cu $2p_{3/2}$ and K-edge regions of the synthesized polymers and the standard Cu^+ complex $[Cu(MeCN)_4]^+$.

polymers ranged from 931.75 to 932.62 eV (Fig. 5a and S15†). These values were lower than that of $[Cu(MeCN)_4]^+$ (933.32 eV),[5a,b] showing that their Cu oxidation state was lower than +1. These results were also confirmed by XANES, with the Cu K-edge energies lying in the range of 8979.00–8979.99 eV ($[Cu(MeCN)_4]^+$: 8981.13 eV)[5a,b] (Fig. 5b and S16†), suggesting that efficient electron transport occurred within the polymeric frameworks.

To evaluate the electronic structures of this series of S–Fe–Cu polymers, the total and partial density of states (DOS) were calculated using the DMol^3 package.[15] In addition to the periodic structures of polymers **1-bpea-2D**, **1-bpee-2D-1·MeCN**, **1-bpee-2D-2**, **1-bpee-2D-3·MeCN**, **1-dpy-2D**, and **1-dpy-1D**, which were derived from their crystallographic data, those of **1-bpp-2D** and **1-bpee-1D** were also proposed and optimized by replacing the chalcogen atoms in the published Se- and Te-containing analogous structures.[5a,b] The DOS plots of these polymers are shown in Fig. S17,† and the contributions of valence and conduction bands are summarized in Table S4.† For the lowest energy-gap polymers, **1-bpea-2D** and **1-bpp-2D**, their valence bands (0 to −2 eV) were dominated mainly by $SFe_3(CO)_9$ and Cu nodes, and the conduction bands were largely contributed from $SFe_3(CO)_9$ with little amounts from the conjugation-interrupted ligands bpea and bpp (Fig. S17 and Table S4†). These results indicated the through-space C–H···O(carbonyl) and aromatic C–H···π interactions that facilitated electron transport in the polymeric framework. Other conjugated dipyridyl-containing polymers showed significant contributions from dipyridyls in the conduction bands, suggesting that both through-bond and through-space electron transports occurred in solid states (Fig. S17 and Table S4†).

Furthermore, the chemical bonding strength around the Cu nodes within these $SFe_3(CO)_9$-based Cu frameworks was investigated through the use of projected crystal orbital Hamilton population (pCOHP) analysis.[16] Generally, negative values of pCOHP indicate the bonding interactions, while positive values indicate the antibonding interactions. The results demonstrated that the Cu–N, Cu–S, Cu–Fe, or Cu–Cu bonding orbitals of polymers **1-bpea-2D**, **1-bpee-2D-1·MeCN**, **1-bpee-2D-2**, **1-bpee-2D-3·MeCN**, **1-dpy-2D**, **1-dpy-1D**, **1-bpp-2D**, and **1-bpee-1D** were localized below the Fermi level of approximately 2.5 eV, while their antibonding orbitals were distributed near the Fermi level (Fig. S18†). It is also noteworthy that the strength of the examined bond can be appraised by utilizing the integrated pCOHP (denoted as ICOHP) situated beneath the Fermi level; a more negative value of ICOHP signifies a stronger bond between two atoms. Relevantly, according to the integrated pCOHP (ICOHP) data, the bond strengths within the aforementioned polymers were found to decrease in the order of Cu–N (−2.07 to −2.40 eV) > Cu–S (−0.49 to −1.65 eV) > Cu–Cu (−0.67 eV) > Cu–Fe (−0.06 to +0.35 eV). Among these, it was noted that the Cu–S bond strength in polymers **1-bpea-2D**, **1-bpee-2D-1·MeCN**, **1-bpee-2D-2**, **1-bpee-2D-3·MeCN**, **1-dpy-2D**, and **1-bpp-2D** varied widely and tended to weaken with the incorporation of more conjugation-interrupted dipyridyl ligands (such as **1-bpp-2D**, −0.49 eV) into the frameworks (Fig. S18†). Conversely, the **L**-type polymer **1-dpy-2D**, one of these $SFe_3(CO)_9$-based polymers, exhibited the strongest Cu–S bond (−1.65 eV), a characteristic that could be correlated with the most efficient through-bond electron transport within its cluster-linked, conjugated dpy-connected framework. Finally, the band structures of these polymers were characterized by flat bands, which were common features in coordination polymers and metal–organic frameworks.[17] These band structure data suggested that the conduction of these polymers could predominantly occur *via* through-space hopping (Fig. S19†).

In summary, these $SFe_3(CO)_9$-based polymers exhibited semiconducting behaviors modulated by coordination modes of cluster $SFe_3(CO)_9$, the choice of dipyridyl ligands, and through-space interactions in the solid state. These new $SFe_3(CO)_9$-based dipyridyl–Cu polymers represent pre-eminent examples of cluster-based conductive polymers, which accelerates the development of molecular devices for semiconducting materials.[18]

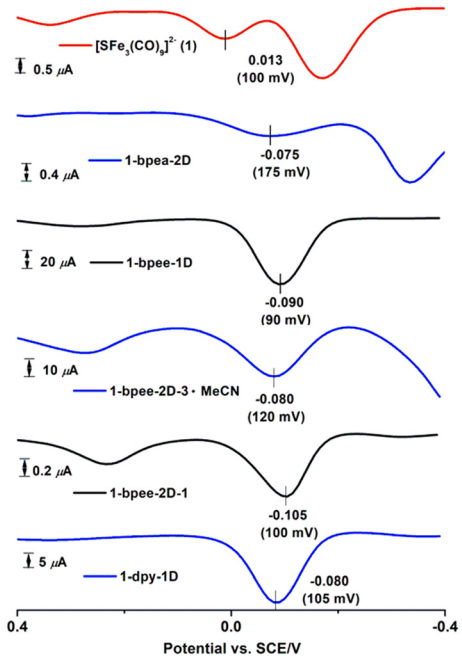

Fig. 6 DPV measurement of $[Et_4N]_2$[**1**],[11] **1-bpea-2D**, **1-bpee-1D**, **1-bpee-2D-3·MeCN**, **1-bpee-2D-1**, and **1-dpy-1D** with the corresponding potentials *versus* a saturated calomel electrode (SCE). Electrolyte, 0.1 M Bu_4NClO_4; working electrode, glassy carbon; scan rate, 100 mV s^{-1}.

Solid-state electrochemical measurements

To examine the potential usage of these $SFe(CO)_9$–dipyridyl Cu polymers in electronic devices, their electrochemical properties were studied by solid-state differential pulse voltammetry (DPV).[19] Polymers **1-bpea-2D** (**L**), **1-bpee-1D** (**B**), **1-bpee-2D-3·MeCN** (**OA**), **1-bpee-2D-1** (**A**), and **1-dpy-1D** (**P**) were selected for the measurement. As shown in Fig. 6 and S20,† the redox patterns of all the selected polymers were found cathodically shifted compared to that of $[Et_4N]_2$[**1**],[11] indicating an increase in the electron density of cluster **1** in the polymeric frameworks. These results concluded that these polymers exhibited accessible redox-active properties in the solid state with significant electron communication within the inorganic cluster $[SFe_3(CO)_9]^{2-}$-based Cu–dipyridyl polymeric backbones. This approach provided ideal synthetic routes for producing redox-active semiconductors with potential applications in batteries, fuel cells, thermoelectrics, supercapacitors, and other related areas.[20]

Conclusion

We applied three-component synthetic routes to a new series of $SFe_3(CO)_9$-based dipyridyl-linked Cu polymers *via* LAG or solution-based approaches. These polymers possessed versatile $SFe_3(CO)_9$ bonding modes, where bpee-connected 2D polymers had unprecedented cluster-armed (**A**) and cluster-one-armed (**OA**) bonding types in chalcogen-containing congeners, mainly attributed to the coordination of the hypervalent μ_5-S atom. Their solid-state structures summarized three fascinating features: **A**- and **OA**-type **1-bpee-2D-1·MeCN**, **1-bpee-2D-2**, and **1-bpee-2D-3·MeCN** displayed parallel-displaced bpee ligands; cluster-linked (**L**) **1-bpea-2D** and **1-dpy-2D** formed four- or five-fold interpenetrating frameworks; all these polymers formed supramolecular networks *via* C–H···O(carbonyl) and C–H···π interactions. Inter-structural transformations of bpee-containing 2D polymers and reversible conversions of bpea- and dpy-containing polymers were achieved by treatment with stoichiometric amounts of dipyridyls or **1**/$[Cu(MeCN)_4]^+$. All the synthesized polymers were found to exhibit tunable semiconducting properties having narrow energy gaps (1.55–1.79 eV) with paralleled electrical conductivities (3.26×10^{-8}–1.48×10^{-6} S cm^{-1}). The pronounced semiconductivities of **L**-type polymers, presumably, originated from the electron-rich $SFe_3(CO)_9$ clusters mainly *via* through-space C–H···O(carbonyl) and C–H···π interactions, resulting in the most efficient electron transport through the dipyridyl–Cu networks. Finally, solid-state electrochemistry was probed to demonstrate that the redox patterns of these $SFe_3(CO)_9$-based polymers were found to be cathodically shifted from those of $[Et_4N]_2$[**1**], revealing that their redox activity was reminiscent of cluster **1** introduced into the Cu–dipyridyl frameworks. These significant findings offered a promising synthetic strategy for producing a new class of $SFe_3(CO)_9$-based Cu–dipyridyl polymers, which would have substantial potential for use as semiconductor materials.

Experimental details

Chemicals and characterization

All LAG reactions were conducted under pure N_2 with AtmosBag (Aldrich), and solution reactions employed standard Schlenk techniques.[21] Solvents were purified, dried, and distilled under N_2 before use. 1,2-bis(4-pyridyl)ethane (bpea) (Aldrich), 4,4′-dipyridyl (dpy) (ACROS), 1,3-bis(4-pyridyl)propane (bpp) (Aldrich), and 1,2-bis(4-pyridyl)ethylene (bpee) (Aldrich) were used as received. $[Et_4N]_2[SFe_3(CO)_9]$[22] and $[Cu(MeCN)_4][BF_4]$[23] were prepared based on published methods. Infrared spectra were recorded with a PerkinElmer Frontier FT-IR spectrometer using an ATR kit. Elemental and TGA analyses were performed on an Elementar Vario analyzer and a TA Q500 (25–900 °C, a heating rate of 5 °C min^{-1} under N_2), respectively, at the NSTC Instrumental Center of National Taiwan University (NTU). PXRD was performed using a Bruker D8 ADVANCE instrument with $Cu_{K\alpha}$ radiation (λ = 1.54050 Å, 40 kV, 40 mA). The topology analysis was performed using the ToposPro package.[24]

Syntheses and structural transformations

Synthesis of $[(\mu_4\text{-S})Fe_3(CO)_9Cu_2(bpea)_2]_n$ (1-bpea-2D). A powder mixture of $[Et_4N]_2$[**1**] (200 mg, 0.28 mmol), $[Cu(MeCN)_4][BF_4]$ (177 mg, 0.56 mmol), and bpea (104 mg, 0.56 mmol) was ground with *ca.* 250 μL of MeCN/DMF (v/v = 2/1) in an agate mortar until the slurry became a powdered sample. The procedure was repeated three times (90 min in total) to ensure that the powdered sample had a similar PXRD pattern to that of **1-bpea-2D**. The sample was washed with H_2O

to obtain the purple-red product **1-bpea-2D** (219 mg, 0.23 mmol; 82% based on $[Et_4N]_2$[**1**]), in which the PXRD pattern matched the simulation generated from the X-ray data of **1-bpea-2D** (Fig. 1a). Crystals of **1-bpea-2D** suitable for X-ray diffraction were produced from MeCN/DMF at 4 °C. Elemental analysis calcd for **1-bpea-2D**: C, 41.84; H, 2.55; N, 5.91. Found: C, 41.59; H, 2.61; N, 5.93. IR (ATR): ν_{CO} = 2015 (vw), 1947 (vs), 1907 (m), 1880 (m), 1854 (s) cm^{-1}.

Synthesis of $[(\mu_5\text{-S})Fe_3(CO)_9Cu_2(bpee)_2]_n$ (1-bpee-2D-1). The process used to synthesize **1-bpea-2D** was applied to the synthesis of **1-bpee-2D-1**, in which $[Et_4N]_2$[**1**] (200 mg, 0.28 mmol), $[Cu(MeCN)_4][BF_4]$ (177 mg, 0.56 mmol), and bpee (102 mg, 0.56 mmol) were used. This LAG reaction was proceeded with *ca.* 750 μL of MeCN (five times, 90 min in total) and then washed with H_2O to give the reddish-brown product **1-bpee-2D-1** (223 mg, 0.24 mmol; 84% based on $[Et_4N]_2$[**1**]) (Fig. 1a). The powdered **1-bpee-2D-1** can be recrystallized in MeCN solution at −30 °C to produce the MeCN-solvated crystals **1-bpee-2D-1·MeCN**. This process was confirmed by checking the unit cell parameters of the crystals of the MeCN-solvated polymer. Elemental analysis calcd for **1-bpee-2D-1**: C, 42.02; H, 2.14; N, 5.94. Found: C, 41.93; H, 2.09; N, 5.93. IR (ATR): ν_{CO} = 2017 (w), 1957 (s), 1938 (m), 1896 (m), 1880 (s), 1839 (m) cm^{-1}.

Synthesis of $[(\mu_5\text{-S})Fe_3(CO)_9Cu_2(bpee)_3]_n$ (1-bpee-2D-2). A MeCN (20 mL) solution of a mixture of $[Et_4N]_2$[**1**] (300 mg, 0.42 mmol), $[Cu(MeCN)_4][BF_4]$ (265 mg, 0.84 mmol), and bpee (231 mg, 1.27 mmol) was stirred in an ice-water bath for 4 h to give a reddish-brown solution. The solvent was filtered, and the residue was washed with H_2O to give the purple-brown product **1-bpee-2D-2** (383 mg, 0.34 mmol; 81% based on $[Et_4N]_2$[**1**]) with the consistent PXRD pattern based on the X-ray data of **1-bpee-2D-2** (Fig. 1b). IR (ATR): ν_{CO} = 2018 (w), 2009 (w), 1952 (m), 1926 (s), 1897 (sh) cm^{-1}. Anal. calcd for **1-bpee-2D-2**: C, 48.02; H, 2.67; N, 7.47. Found: C, 47.61; H, 2.56; N, 7.43. Crystals of **1-bpee-2D-2** suitable for X-ray diffraction were produced from MeCN at −30 °C.

Synthesis of $[(\mu_5\text{-S})Fe_3(CO)_9Cu_2(bpee)_{3.5}\cdot MeCN]_n$ (1-bpee-2D-3·MeCN). The process used to synthesize **1-bpea-2D** was applied to the synthesis of **1-bpee-2D-3·MeCN**, in which $[Et_4N]_2$[**1**] (200 mg, 0.28 mmol), $[Cu(MeCN)_4][BF_4]$ (177 mg, 0.56 mmol), and bpee (180 mg, 0.98 mmol) were used. This LAG reaction was proceeded with *ca.* 750 μL of MeCN (five times, 90 min in total) and then washed with H_2O to give the reddish-brown product **1-bpee-2D-3·MeCN** (266 mg, 0.21 mmol; 75% based on $[Et_4N]_2$[**1**]). The experimental PXRD pattern was consistent with that simulated from the X-ray data of **1-bpee-2D-3·MeCN** (Fig. 1b). Crystals of **1-bpee-2D-3·MeCN** suitable for X-ray diffraction were produced from MeCN at −30 °C. Anal. calcd for **1-bpee-2D-3·MeCN**: C, 50.62; H, 3.05; N, 8.91. Found: C, 48.87; H, 2.99; N, 8.55. IR (ATR): ν_{CO} = 2007 (w), 1932 (m), 1927 (m), 1907 (s), 1896 (sh), 1886 (m), 1873 (s) cm^{-1}.

Conversion of 1-bpea-1D to 1-bpea-2D. A mixture of a powder sample of **1-bpea-1D** (112 mg, 0.15 mmol based on the $[(\mu_3\text{-S})Fe_3(CO)_9Cu_2(bpea)]$ unit) and bpea (27 mg, 0.15 mmol) was ground with *ca.* 150 μL of MeCN/DMF (v/v = 2/1) until the slurry became a powder sample of **1-bpea-2D**, which was produced in a quantitative yield with the consistent PXRD pattern based on the X-ray data of **1-bpea-2D** (Fig. S2a†).

Conversion of 1-bpea-2D to 1-bpea-1D. A mixture of **1-bpea-2D** (101 mg, 0.11 mmol based on the $[(\mu_4\text{-S})Fe_3(CO)_9Cu_2(bpea)_2]$ unit), $[Et_4N]_2$[**1**] (75 mg, 0.11 mmol), and $[Cu(MeCN)_4][BF_4]$ (67 mg, 0.21 mmol) was ground with *ca.* 450 μL of THF/Et_2O (v/v = 1/1, three times, 1.5 h in total) and then washed with H_2O to give a powder sample of **1-bpea-1D** (141 mg, 0.19 mmol based on the $[SFe_3(CO)_9Cu_2(bpea)]$ unit; 86%) with the consistent PXRD pattern based on the X-ray data of $[TeFe_3(CO)_9Cu_2(bpea)]_n$ (Fig. S2b†).[5b]

Conversion of 1-bpee-2D-1 to 1-bpee-2D-3·MeCN. The conversion process of **1-bpea-1D** to **1-bpea-2D** was applied to the transformation of **1-bpee-2D-1** into **1-bpee-2D-3·MeCN**. As-synthesized **1-bpee-2D-1** (151 mg, 0.16 mmol based on the $[(\mu_5\text{-S})Fe_3(CO)_9Cu_2(bpee)_2]$ unit) and bpee (43.7 mg, 0.24 mmol) was ground with *ca.* 500 μL of MeCN until the slurry became a powder sample of **1-bpee-2D-3·MeCN**, which is produced in a quantitative yield with the consistent PXRD pattern based on the X-ray data of **1-bpee-2D-3·MeCN** (Fig. S3a†).

Conversion of 1-bpee-2D-3·MeCN to 1-bpee-2D-1. The process used to convert **1-bpea-2D** to **1-bpea-1D** was applied to the transformation of **1-bpee-2D-3·MeCN** into **1-bpee-2D-1**, in which **1-bpee-2D-3·MeCN** (130 mg, 0.11 mmol based on the $[(\mu_5\text{-S})Fe_3(CO)_9Cu_2(bpee)_{3.5}]$ unit), $[Et_4N]_2$[**1**] (56.8 mg, 0.08 mmol), and $[Cu(MeCN)_4][BF_4]$ (50.6 mg, 0.16 mmol) were used. This LAG reaction was proceeded with *ca.* 500 μL of MeCN (eight times, 1.5 h in total) and then washed with H_2O to give **1-bpee-2D-1** (154 mg, 0.16 mmol based on the $[(\mu_5\text{-S})Fe_3(CO)_9Cu_2(bpee)_2]$ unit; 84%). The experimental PXRD pattern was consistent with that of the as-synthesized powder of **1-bpee-2D-1** (Fig. S3b†).

Author contributions

M.-C. Hsu: investigation, formal analysis, validation, visualization, and writing – original draft; R. Y. Lin: investigation and formal analysis; T.-Y. Sun: investigation and formal analysis; Y.-X. Huang: investigation and formal analysis; M.-S. Li: investigation and formal analysis; Y.-H. Li: conceptualization, visualization, and writing – review & editing; H.-L. Chen: resources, software, and writing – review & editing; M. Shieh: supervision, conceptualization, and writing – review & editing.

Conflicts of interest

There are no conflicts to declare.

Acknowledgements

This work was sponsored by the National Science and Technology Council of Taiwan (NSTC 112-2113-M-003-011-MY2 to M. S.). The authors wish to show gratitude to the National Synchrotron Radiation Research Center (NSRRC) of Taiwan for

XAS measurements and the National Center for High-Performance Computing (NCHC) of Taiwan for providing the computing time. Ms W.-L. Chen and Mr W.-M. Ke are acknowledged for some preliminary results.

References

1 (*a*) S. R. Batten, S. M. Neville and D. R. Turner, *Coordination polymers: design, analysis and application*, Royal Society of Chemistry, 2008; (*b*) J. W. Steed and J. L. Atwood, *Supramolecular chemistry*, John Wiley & Sons, 2022; (*c*) J. Xie, L. Wang and J. S. Anderson, *Chem. Sci.*, 2020, **11**, 8350–8372; (*d*) L. Carlucci, G. Ciani, D. M. Proserpio, T. G. Mitina and V. A. Blatov, *Chem. Rev.*, 2014, **114**, 7557–7580; (*e*) H. Furukawa, K. E. Cordova, M. O'Keeffe and O. M. Yaghi, *Science*, 2013, **341**, 1230444; (*f*) G. K. Kole and J. J. Vittal, *Chem. Soc. Rev.*, 2013, **42**, 1755–1775; (*g*) W. L. Leong and J. J. Vittal, *Chem. Rev.*, 2011, **111**, 688–764; (*h*) U. Schubert, *Chem. Soc. Rev.*, 2011, **40**, 575–582.

2 (*a*) M. Shieh and Y.-H. Li, in *Chalcogen Chemistry: Fundamentals and Applications*, ed. V. Lippolis, C. Santi, E. J. Lenardão and A. L. Braga, Royal Society of Chemistry, 2023, pp. 1–26; (*b*) M. Shieh, Y.-H. Liu, Y.-H. Li and R. Y. Lin, *CrystEngComm*, 2019, **21**, 7341–7364; (*c*) M. Shieh, Y.-H. Li and M.-C. Hsu, *J. Chin. Chem. Soc.*, 2023, **70**, 984–991; (*d*) M. Shieh and C.-C. Yu, *J. Organomet. Chem.*, 2017, **849**, 219–227.

3 (*a*) P. Braunstein, L. A. Oro and P. R. Raithby, *Metal Clusters in Chemistry*, Wiley-VCH, Weinheim, 1999; (*b*) D. F. Shriver, H. D. Kaesz and R. D. Adams, *The Chemistry of metal cluster complexes*, VCH, New York, 1990; (*c*) M. Shieh, C.-Y. Miu, Y.-Y. Chu and C.-N. Lin, *Coord. Chem. Rev.*, 2012, **256**, 637–694; (*d*) C. Cesari, J.-H. Shon, S. Zacchini and L. A. Berben, *Chem. Soc. Rev.*, 2021, **50**, 9503–9539; (*e*) K. H. Whitmire, *Coord. Chem. Rev.*, 2018, **376**, 114–195.

4 (*a*) P. A. Shelyganov, M. Elsayed Moussa, M. Seidl and M. Scheer, *Chem. – Eur. J.*, 2023, **29**, e202300610; (*b*) M. Elsayed Moussa, P. A. Shelyganov, M. Seidl, E. Peresypkina, N. Berg, R. M. Gschwind, G. Balázs, J. Schiller and M. Scheer, *Chem. – Eur. J.*, 2021, **27**, 5028–5034; (*c*) M. Elsayed Moussa, M. Fleischmann, E. V. Peresypkina, L. Dutsch, M. Seidl, G. Balazs and M. Scheer, *Eur. J. Inorg. Chem.*, 2017, 3222–3226; (*d*) B. Attenberger, E. V. Peresypkina and M. Scheer, *Inorg. Chem.*, 2015, **54**, 7021–7029; (*e*) J. Bai, E. Leiner and M. Scheer, *Angew. Chem., Int. Ed.*, 2002, **41**, 783–786.

5 (*a*) Y.-H. Liu, K.-T. Huang, W.-C. Chen, Y.-W. Li, W.-M. Ke, B.-R. Ho, M.-C. Hsu, Y.-H. Li and M. Shieh, *Inorg. Chem.*, 2021, **60**, 18270–18282; (*b*) M. Shieh, C.-C. Yu, C.-Y. Miu, C.-H. Kung, C.-Y. Huang, Y.-H. Liu, H.-L. Liu and C.-C. Shen, *Chem. – Eur. J.*, 2017, **23**, 11261–11271; (*c*) M. Shieh, C.-H. Ho, W.-S. Sheu, B.-G. Chen, Y.-Y. Chu, C.-Y. Miu, H.-L. Liu and C.-C. Shen, *J. Am. Chem. Soc.*, 2008, **130**, 14114–14116; (*d*) C.-N. Lin, W.-T. Jhu and M. Shieh, *Chem. Commun.*, 2014, **50**, 1134–1136; (*e*) M. Shieh, Y.-H. Li, Y.-H. Chang, K.-S. Lu, C.-N. Lin and B.-R. Ho, *J. Organomet. Chem.*, 2023, **1001**, 122884; (*f*) M. Shieh, M.-H. Hsu, W.-S. Sheu, L.-F. Jang, S.-F. Lin, Y.-Y. Chu, C.-Y. Miu, Y.-W. Lai, H.-L. Liu and J. L. Her, *Chem. – Eur. J.*, 2007, **13**, 6605–6616.

6 T. Friščić, C. Mottillo and H. M. Titi, *Angew. Chem.*, 2020, **132**, 1030–1041.

7 R. H. Crabtree, *Chem. Soc. Rev.*, 2017, **46**, 1720–1729.

8 (*a*) M. O'Keeffe, M. A. Peskov, S. J. Ramsden and O. M. Yaghi, *Acc. Chem. Res.*, 2008, **41**, 1782–1789; (*b*) S. R. Batten and R. Robson, *Angew. Chem., Int. Ed.*, 1998, **37**, 1460–1494.

9 (*a*) D. Braga and F. Grepioni, *Acc. Chem. Res.*, 1997, **30**, 81–87; (*b*) D. Braga, F. Grepioni, K. Biradha, V. Pedireddi and G. R. Desiraju, *J. Am. Chem. Soc.*, 1995, **117**, 3156–3166.

10 (*a*) E. R. Tiekink and J. Zukerman-Schpector, *The importance of pi-interactions in crystal engineering: Frontiers in Crystal Engineering*, John Wiley & Sons, 2012; (*b*) K. Biradha and M. J. Zaworotko, *J. Am. Chem. Soc.*, 1998, **120**, 6431–6432.

11 C.-Y. Miu, H.-H. Chi, S.-W. Chen, J.-J. Cherng, M.-H. Hsu, Y.-X. Huang and M. Shieh, *New J. Chem.*, 2011, **35**, 2442–2455.

12 (*a*) P. Kubelka, *Z. Technol. Phys.*, 1931, **12**, 593–601; (*b*) J. Tauc, *Mater. Res. Bull.*, 1970, **5**, 721–729.

13 (*a*) L. S. Xie, G. Skorupskii and M. Dincă, *Chem. Rev.*, 2020, **120**, 8536–8580; (*b*) L. Sun, S. S. Park, D. Sheberla and M. Dincă, *J. Am. Chem. Soc.*, 2016, **138**, 14772–14782.

14 T.-H. Le, Y. Kim and H. Yoon, *Polymers*, 2017, **9**, 150.

15 (*a*) B. Delley, *J. Chem. Phys.*, 2000, **113**, 7756–7764; (*b*) B. Delley, *J. Chem. Phys.*, 1990, **92**, 508–517.

16 R. Dronskowski and P. E. Blöchl, *J. Chem. Phys.*, 1993, **97**, 8617–8624.

17 (*a*) L. M. Yang, P. Ravindran, P. Vajeeston and M. Tilset, *J. Mater. Chem.*, 2012, **22**, 16324–16335; (*b*) L. M. Yang, P. Ravindran and M. Tilset, *Inorg. Chem.*, 2013, **52**, 4217–4228; (*c*) L. M. Yang, G. Y. Fang, J. Ma, E. Ganz and S. S. Han, *Cryst. Growth Des.*, 2014, **14**, 2532–2541.

18 (*a*) V. Rubio-Giménez, S. Tatay and C. Martí-Gastaldo, *Chem. Soc. Rev.*, 2020, **49**, 5601–5638; (*b*) L.-P. Tang, S. Yang, D. Liu, C. Wang, Y. Ge, L.-M. Tang, R.-L. Zhou and H. Zhang, *J. Mater. Chem. A*, 2020, **8**, 14356–14383; (*c*) G. Givaja, P. Amo-Ochoa, C. J. Gomez-Garcia and F. Zamora, *Chem. Soc. Rev.*, 2012, **41**, 115–147; (*d*) S. Horike, D. Umeyama and S. Kitagawa, *Acc. Chem. Res.*, 2013, **46**, 2376–2384; (*e*) A. Nafady, A. P. O'Mullane and A. M. Bond, *Coord. Chem. Rev.*, 2014, **268**, 101–142; (*f*) G. H. Morritt, H. Michaels and M. Freitag, *Chem. Phys. Rev.*, 2022, **3**, 011306.

19 D. Kim, S. Lee and Y. Piao, *J. Electroanal. Chem.*, 2017, **794**, 221–228.

20 (*a*) I. Stassen, N. Burtch, A. Talin, P. Falcaro, M. Allendorf and R. Ameloot, *Chem. Soc. Rev.*, 2017, **46**, 3185–3241; (*b*) N. E. Horwitz, J. Xie, A. S. Filatov, R. J. Papoular, W. E. Shepard, D. Z. Zee, M. P. Grahn, C. Gilder and J. S. Anderson, *J. Am. Chem. Soc.*, 2019, **141**, 3940–3951;

(*c*) D. Sheberla, J. C. Bachman, J. S. Elias, C.-J. Sun, Y. Shao-Horn and M. Dincă, *Nat. Mater.*, 2017, **16**, 220–224; (*d*) X. Zhou, Y. Yu, J. Yang, H. Wang, M. Jia and J. Tang, *ChemElectroChem*, 2019, **6**, 2056–2063; (*e*) Y. Kamakura, S. Fujisawa, K. Takahashi, H. Toshima, Y. Nakatani, H. Yoshikawa, A. Saeki, K. Ogasawara and D. Tanaka, *Inorg. Chem.*, 2021, **60**, 12691–12695.

21 D. F. Shriver and M. A. Drezdzon, *The manipulation of air-sensitive compounds*, John Wiley & Sons, 1986.

22 J.-J. Cherng, Y.-C. Tsai, C.-H. Ueng, G.-H. Lee, S.-M. Peng and M. Shieh, *Organometallics*, 1998, **17**, 255–261.

23 (*a*) G. J. Kubas, *Inorg. Synth.*, 1979, **19**, 90–92; (*b*) M. G. Simmons, C. L. Merrill, L. J. Wilson, L. A. Bottomley and K. M. Kadish, *J. Chem. Soc., Dalton Trans.*, 1980, 1827–1837.

24 V. A. Blatov, A. P. Shevchenko and D. M. Proserpio, *Cryst. Growth Des.*, 2014, **14**, 3576–3586. ToposPro is available at **https://www.topospro.com**.